Aerodynamic Design Analysis of the HEXAFLY-INT Hypersonic Glider

Giuseppe Pezzella[1], Marco Marini[2]
CIRA, Italian Aerospace Research Center, Via Maiorise, 81043 Capua (CE), Italy

Bodo Reimann[3],
German Aerospace Center (DLR), Lilienthalplatz 7, 38108 Braunschweig, Germany

and

Johan Steelant[4]
ESA-ESTEC, European Space Agency, Keplerlaan 1, 2200 AZ Noordwijk, The Netherlands

This paper deals with the aerodynamic performance analysis of the expendable Experimental Flight Test Vehicle under development in the seventh framework programme, namely HEXAFLY-INT. A mission scenario, the different flight segments and events to which the payload is exposed to are described and justified. This allowed the definition of the aero-thermo-mechanical loads required to conceptually design all elements on board of the vehicle. This flying test bed is a self-controlled glider configuration that shall face a hypersonic flight starting at about Mach 8, just after the separation from the experimental support module at about 50 km altitude, up to vehicle loss. During this flight, several experiments shall be carried out. The appraisal of the vehicle aerodynamic performance is needed for Flight Mechanics and Guidance, Navigation and Control analysis. In particular, hinge line moments for the EFTV's aileron are also addressed to design the actuation line and to select the actuator device itself. The vehicle made maximum use of databases, expertise, technologies and materials elaborated in previously European community co-funded projects ATLLAS I & II, LAPCAT I & II, and HEXAFLY.

Nomenclature

AoA	=	angle of attack
AoS	=	angle of sideslip
b	=	wing span
C_A	=	axial force coefficient
C_D	=	drag force coefficient
C_h	=	hinge-moment coefficient
C_L	=	lift force coefficient
C_N	=	normal force coefficient
C_Y	=	side force coefficient
C_l	=	rolling moment (=Cmx)
C_m	=	pitching moment (=Cmy)
C_n	=	yawing moment (=Cmz)
D	=	aerodynamic drag, diameter
E	=	lift-to-drag ratio (aerodynamic efficiency)
H, h	=	altitude, height

[1] Ph. D., Research Engineer, Aerothermodynamic Section, Analysis and Extrapolation to Flight Lab., Head. g.pezzella@cira.it.
[2] Ph. D., Senior Research Engineer, Space Technology Integration and Demonstrators Unit, m.marini@cira.it.
[3] Ph. D., Researcher, Institute of Aerodynamics and Flow Technology | Spacecraft, Bodo.Reimann@dlr.de.
[4] PhD, Senior Research Engineer, ESA-ESTEC, Aerothermodynamics and Propulsion Analysis Section TEC-MPA, P.O. Box 299, Noordwijk, Netherlands, Johan.Steelant@esa.int, AIAA Member.

H_0 = total enthalpy
HF = heat flux
Kn = Knudsen number
L = length, aerodynamic lift, vehicle length
L/D = aerodynamic efficiency (E_{ff})
M = Mach number, pitching moment, mass
N = normal force
P = pressure
q = heat flux
R = gas constant
Re = Reynolds number
S = surface
T = temperature
u, v, w = velocity components
V = velocity, volume
X,Y,Z = coordinates

Greek Symbols
α = angle of attack
β = angle of sideslip
Δ = variation
δ = aileron deflection
ε = emissivity coefficient
γ = specific heats ratio
λ = molecular mean free path
Λ = wing sweep angle
φ = roll angle
ω = angular speed
ρ = density
τ = shear stress

Subscript
a = aileron
dyn = dynamic
e = elevon, edge of boundary layer
$flap$ = aileron related
$hinge$ = hinge-line related
Ref = reference
t = transition
∞ = free stream conditions

I. Introduction

Over the last years, innovative concepts of civil high-speed transportation vehicles were proposed[1,2]. These vehicles have a strong potential to increase the cruise range efficiency at high Mach numbers, thanks to efficient propulsion units (turbojets based on air-turbo-rocket cycle for take-off and landing, and dual-mode ramjet/scramjet for cruise) combined with high-lifting vehicle concepts. Nonetheless, performing a flight test will be the only and ultimate proof to demonstrate the technical feasibility of these new promising concepts and would result into a major breakthrough in high-speed flight[3].

In this frame the HEXAFLY-INT project, funded by European Commission by means of 7th Framework Programme, intends to test in free-flight conditions an innovative (unpowered) gliding high-speed vehicle with several breakthrough technologies on-board[4]. This approach will create the basis to gradually increase the readiness level of a consistent number of technologies suitable for high-speed flying systems. The vehicle, namely Experimental Flight Test Vehicle (EFTV), will be launched by a sounding rocket in a suborbital trajectory having an apogee at around 90 km, as shown in Figure 1. After the release from the launcher, the EFTV will perform the early descent flight docked to a service module, namely the Experimental Service Module (ESM). This latter has the aim to control vehicle attitude by means of a cold gas system (CGS) when dynamic pressure does not allow controlling the vehicle by aerodynamic surfaces.

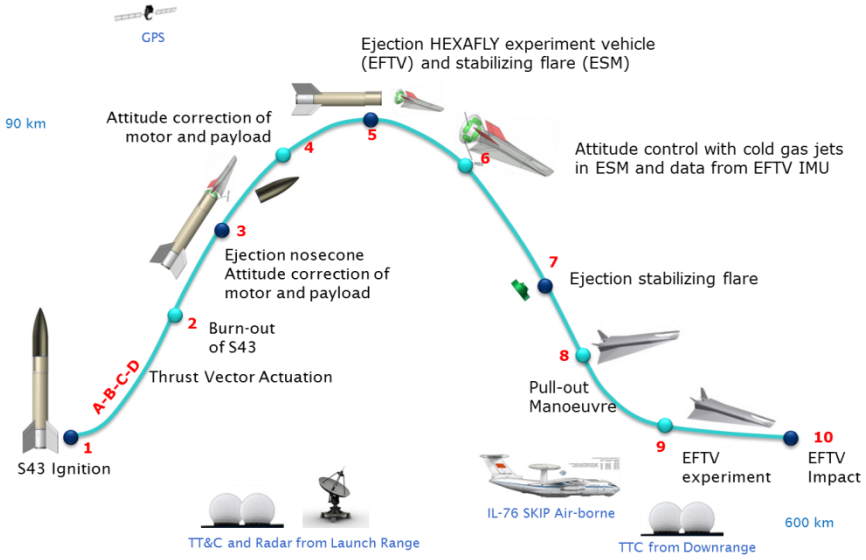

Figure 1. Flight trajectory for the EFTV.

As soon as EFTV features complete aerodynamic control authority, it undocks from ESM and flies up to perform a hypersonic cruise at about Mach 7. In this phase, namely the experimental window, the free-flying vehicle (i.e. EFTV) will allow to demonstrate a high aerodynamic efficiency, a positive aerodynamic balance at controlled cruise Mach numbers, an optimal use of advanced high-temperature materials and structures, and potentially the evaluation of the sonic boom impact by deploying dedicated ground measurement equipment.

II. Vehicle Configuration

The overall aim of the HEXAFLY-INT project is to design, manufacture and test in flight a high speed gliding vehicle, based on the configuration developed in previously European community (EC) co-funded projects ATLLAS I & II, LAPCAT I & II, and HEXAFLY[1,5,6]. Under HEXAFLY-INT the flight experiment is focused on a self-controlled glider configuration[7].

The EFTV vehicle configuration is reported in Figure 2, where the train (i.e. EFTV docked to ESM) and ESM configurations are provided as well[8].

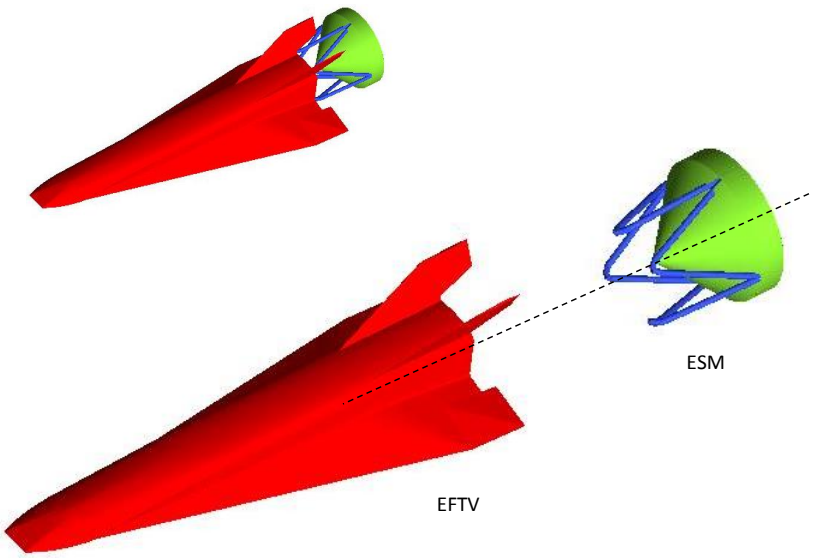

Figure 2. EFTV docked to ESM, EFTV and ESM aeroshapes.

The vehicle design makes maximum use of databases, expertise, technologies and materials elaborated in previously European community co-funded projects ATLLAS I & II, LAPCAT I & II, and HEXAFLY. [1-3]

The prime objectives of this free-flight experiment are: to demonstrate high aerodynamic efficiency in combination with high internal volume; controlled level flight at a cruise Mach number of 7 to 8; optimal use of advanced high-temperature materials and/or structures; an evaluation of the sonic boom impact by deploying dedicated ground measurement equipment.

In this framework, the appraisal of aerodynamic performance of the vehicle glider is mandatory in order to fulfil mission requirements[9,10,11]. In particular, the present research effort focuses attention on several CFD simulations performed to assess vehicle aerodynamic performances. Results of both Eulerian and Navier-Stokes (both in laminar and turbulent flow conditions) simulations, carried out at different Mach number and glider attitude, are provided and discussed in the paper. These CFD results allowed also assessing the flight attitude conditions of the natural trim point the EFTV features and the static stability conditions as well. These conditions are fundamental for the design and sizing of the Flight Control System (FCS).

III. Reference Mission Scenario

The reference mission scenario currently foreseen for the EFTV+ESM, and EFTV design is summarized from Figure 3 to Figure 5. The HEXAFLY-INT mission is conceived to achieve a hypersonic levelled flight at an altitude of about 30 km, while being injected from a semi-ballistic trajectory depicted in Figure 3, and described below.[4]

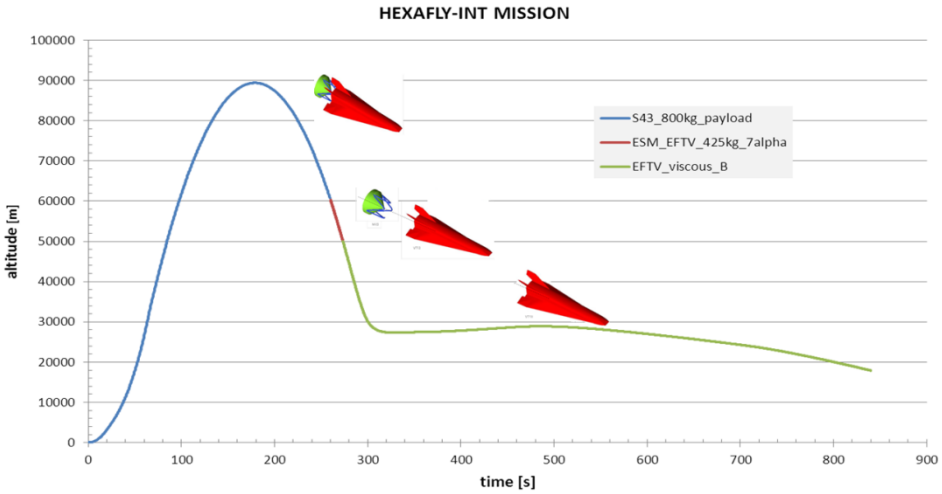

Figure 3. Overall altitude time history.

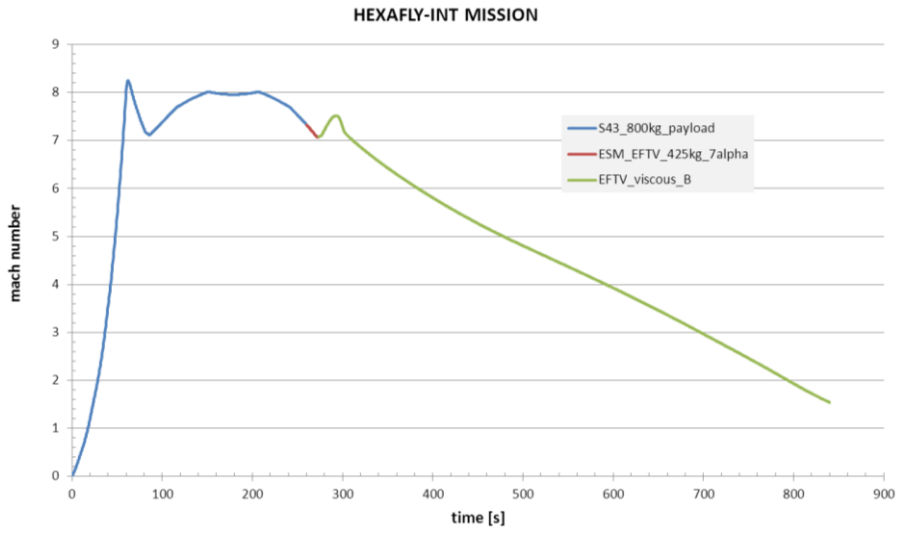

Figure 4. Overall Mach number time history.

After a boost provided by an expendable launch vehicle equipped by a solid rocket motor (S43), bringing the scientific payload (EFTV+ESM) to about 90 km apogee, it follows a ballistic phase in the high atmosphere stabilized by an attitude control system, through CGS, in combination with an aerodynamic flare (ESM). [4] The vehicle (EFTV) is detached from the ESM when ESM-EFTV separation conditions are reached, i.e. at 50km altitude. After the separation a pull-out manoeuver brings EFTV to a hypersonic levelled flight at a target altitude of about 30 km. The Mach number time history is shown in Figure 4; while the overall time histories of AoA and aileron trim deflections are provided in Figure 5.

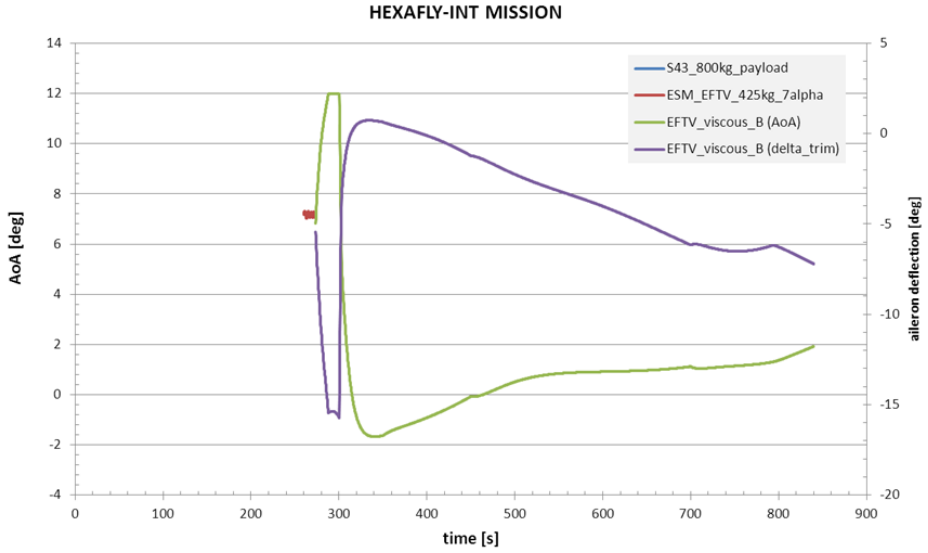

Figure 5. Overall time histories of AoA and aileron trim deflection.

Note that the trajectories have been generated by DLR-Moraba for what concerns the launch vehicle, assuming a total payload weight of 800 kg (EFTV, ESM, launch vehicle service module, fairing) for the S43 booster, and by Gas Dynamics Ltd. (GDL, partner of HEXAFLY-INT project) for the EFTV+ESM from 60 km to 50 km altitude, and for the EFTV after the separation from ESM, from 50 km to about 20 km altitude.[9]

A. Flight regime assessment

Generally speaking, during a re-entry, a vehicle can experience three main flow regimes according to Bird's classification.[12] During the upper part of descent trajectory, one is faced with the free molecular and the transitional flow regime, whereas a continuum flow regime is experienced within the lower atmospheric layers (see Figure 6).

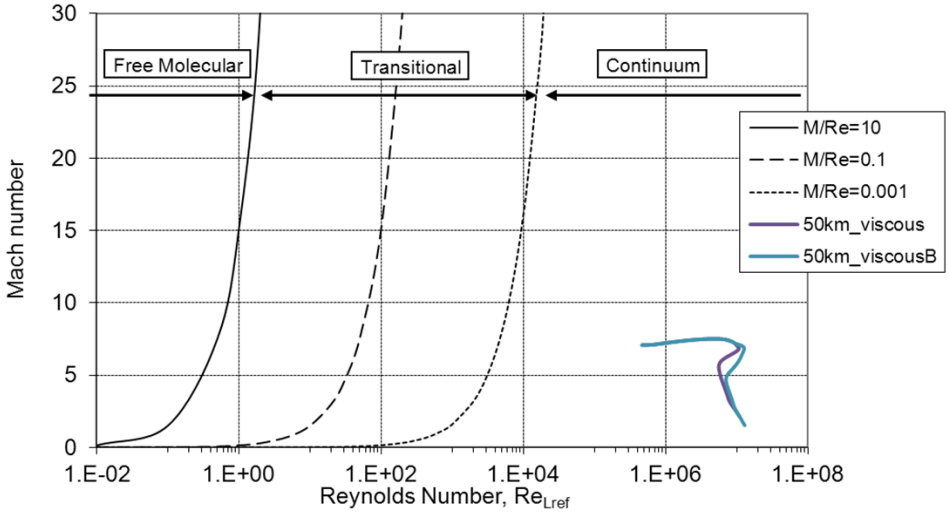

Figure 6. Flight regime assessment.

This figure provides the EFTV flight envelope (two trajectories) in the Mach-Reynolds numbers map. The similarity parameter governing these different flow regimes is the Knudsen number, defined as (rarefaction parameter):

$$Kn_{\infty L_{ref}} = \frac{\lambda}{L_{ref}} = 1.25\sqrt{\gamma}\frac{M_\infty}{Re_{\infty L_{ref}}} \tag{1}$$

where L_{ref} is the characteristic length of the body and λ is the molecular mean free path. As shown in Figure 6, the region for $10^{-3} < Kn_\infty < 10$ is the rarefied-flow transition region. Figure 6 points out clearly that only continuum flow conditions are expected for the EFTV throughout its mission. As a consequence, the glider aerodynamic appraisal will be addressed for continuum flow conditions only.The EFTV flight envelope in the altitude-velocity map is shown Figure 7, where iso-Mach and iso-Reynolds curves are also provided to allow defining vehicle aerodynamics.[10,11,12,13]

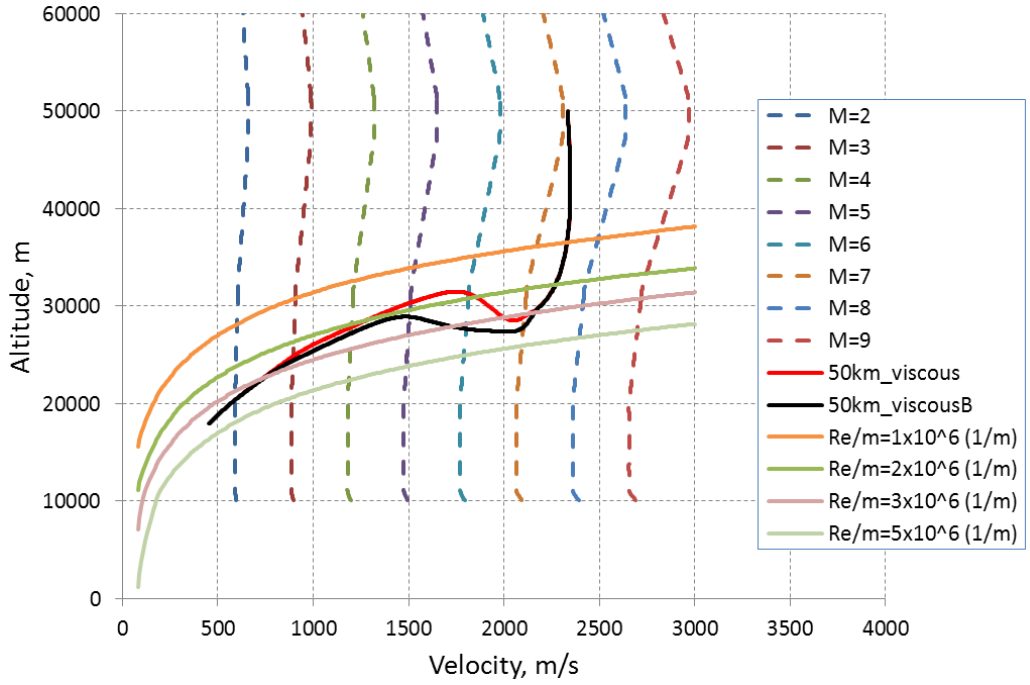

Figure 7. Mach-Reynolds grid in the altitude-velocity map.

IV. Description of Aerodynamic Design Approach and Used Tools

A summary review of the aerodynamic characteristics of the EFTV glider concept is performed. These evaluations are aimed only to carry out a preliminary AErodynamic DataBase (AEDB) for such configuration with the goal to provide aerodynamic database for the Flight Mechanics analyses. In fact, it must be verified that vehicle aerodynamic surfaces are able to provide lift at hypersonic atmospheric entry to stay within the load constraints during descent.

A. Aerodynamic design approach

Glider aerodynamic coefficients have been provided as a function of Mach number, angle of attack, sideslip angle, and aileron deflections, according to the Trajectory-Based design approach.[12] This design approach consists in performing the aerodynamic/aerothermal computations at a finite number of "critical" points on a given design trajectory, as sketched in Figure 8. In particular, the AEDB was setup by performing a massive number of Eulerian CFD (inviscid) computations, in order to focus on some critical design aspects not predictable with simplified tools. Solving the Euler governing equations requires less elements in a spatial grid dimension (e.g. no boundary layer at wall) than solving the full Navier-Stokes equations, thus demanding a significantly lower computational effort.

Euler method does not account for viscosity effects but is sufficient for prediction of surface pressure distribution, position and intensity of shock-shock wave interactions.

At the present stage, viscous effects on vehicle aerodynamics have been assessed only at engineering level and through a limited number of Navier-Stokes computations.

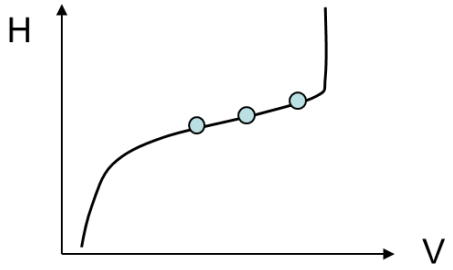

Figure 8. Trajectory-based design approach in the Altitude-Velocity map.

The range between Mach 2 and Mach 9 was analysed for the EFTV in standalone configuration. In particular, only continuum regime (supersonic and hypersonic speed ranges), with the air modelled as an ideal gas, has been considered. Even though CFD simulations are carried out at hypersonic flow conditions, the ideal gas assumption was still valid considering that the higher Mach number, here considered, is equal to 9 and, in particular, because of the EFTV aeroshape features a very slender configuration (leading edge radius of 2 mm for nosetip, wings and fins) that shall fly at rather low angle of attack (i.e. with weak attached shock waves).

In the following paragraphs the tools used for the analysis are described more in detail.

B. Aerodynamic analysis tools

So far, the numerical code used by CIRA to carry out CFD analyses of the HEXAFLY-INT vehicle glider is the commercial code ANSYS FLUENT® Vs. 14. It solves the Reynolds Averaged Navier-Stokes (RANS) equations, including chemical and vibrational non-equilibrium, on hybrid grids by means of the Finite Volume approach. FLUENT® uses a Flux Difference Splitting (FDS) second order upwind scheme for the spatial reconstruction of convective terms, while for the diffusive fluxes a cell-centred scheme is applied. An alternative way to compute the flux vector is also available by using a flux-vector splitting scheme, namely Advection Upstream Splitting Method (AUSM). AUSM provides exact resolution of contact and shock discontinuities and it is less susceptible to the numerical instability known as "carbuncle" phenomenon. Implicit solver formulation is available and considered in the computations of this work. Indeed, due to broader stability characteristics of the implicit formulation, a converged steady-state solution can be obtained much faster using the implicit formulation rather than the explicit formulation. Global transport properties of the gas mixture rely on semi-empirical rules such as Wilke's mixing rule for viscosity and thermal conductivity. The viscosity and thermal conductivity of i^{th} species is obtained by kinetic theory of gases. For the diffusion coefficient of the i^{th} species in the mixture the multi-component diffusion coefficient is applied, where species mass diffusivity is evaluated by kinetic theory. The two-equation SST k-ω model has been considered to account for turbulence effects. Also a parallel version of the code is currently available.

Finally, aerodynamic design analyses carried out by DLR were performed by using the in-house DLR TAU code[14]. This flow solver is a finite volume method. Based on the primary grid an edge based metric called dual grid is generated in a preprocessing step. If multi-grid technique is used, the preprocessor also agglomerates coarser levels of the dual grid. In the case of parallel computations domain splitting is also done by the preprocessor. For time discretization, including local time stepping, a three dimensional Runge-Kutta, as well as an implicit approximately factored LU-SGS scheme is implemented. For supersonic flows the AUSMDV upwind scheme with MUSCLE (Monotonic Upstream-Centered Scheme for Conservation Laws) reconstruction is used to compute the inviscid fluxes.

In the present study the TAU's inviscid ideal gas solver (γ=1.4, R=287 J/kg/K) was applied. The primary mesh for a simulation of half configuration with symmetry plane consists of about 9 million tetrahedrons.

V. Aerodynamic Analysis

The aerodynamic analysis of EFTV is reported hereinafter in term of lift (C_L), drag (C_D), side force (C_Y), rolling moment (C_l), pitching moment (C_m), and yawing moment (C_n) coefficients, which are calculated according to the following equations.

$$C_i = \frac{F_i}{\frac{1}{2}\rho_\infty V_\infty^2 S_{ref}} \qquad i = L, D, Y \tag{2}$$

$$C_l = \frac{M_x}{\frac{1}{2}\rho_\infty V_\infty^2 b_{ref} S_{ref}} \tag{3}$$

$$C_m = \frac{M_y}{\frac{1}{2}\rho_\infty V_\infty^2 L_{ref} S_{ref}} \tag{4}$$

$$C_n = \frac{M_z}{\frac{1}{2}\rho_\infty V_\infty^2 b_{ref} S_{ref}} \tag{5}$$

The moment reference centre (MRC) for the calculation of the aerodynamic moment coefficients is shown in Figure 9 with respect to the Layout Reference Frame (LRF).

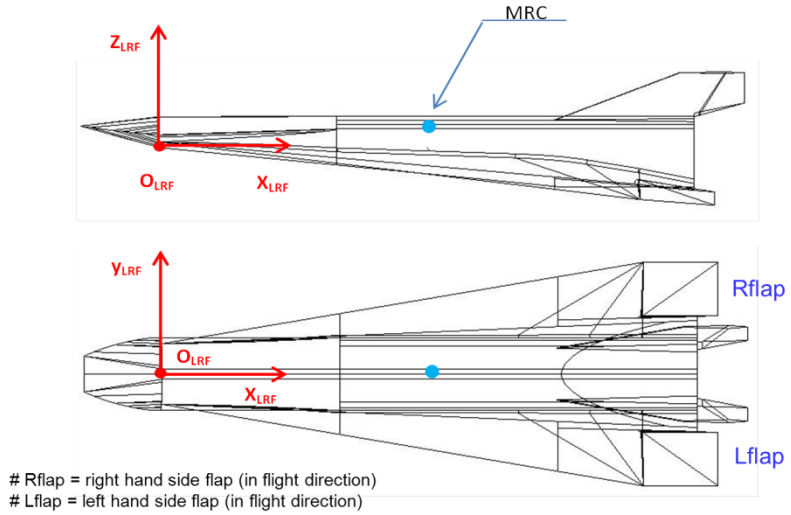

Figure 9. The Layout Reference Frame.

Thus, the MRC coordinates in LRF for the EFTV are (1.455, 0, 0.120) [m]. In particular, C_L and C_D are provided in the vehicle's wind reference frame (WRF), while C_Y, C_l, C_m, and C_n are evaluated in the vehicle's body reference frame (BRF) shown in Figure 10.

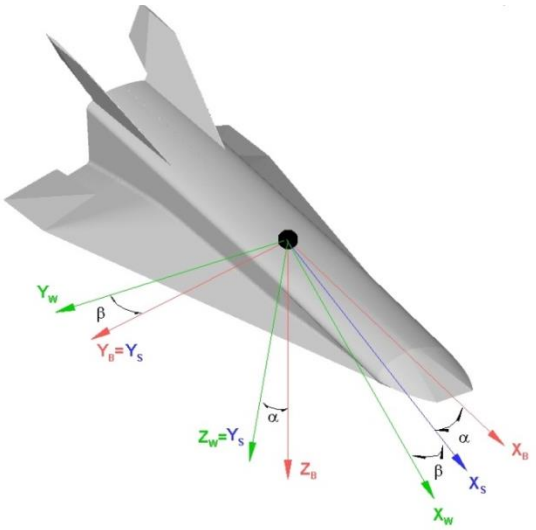

Figure 10. The wind reference frame (X_w,Y_w,Z_w) and the body reference frame (X_B,Y_B,Z_B).

A. General inputs for aerodynamic data set generation

The following reference parameters have been considered for the generation of the aerodynamic data set of EFTV (see Figure 11): L_{ref}=3.29 m (e.g. body length – longitudinal reference length); b_{ref}=1.24 m (e.g. wing span – lateral-directional reference length); S_{ref}=2.52 m^2 (e.g. vehicle planform area – reference area).

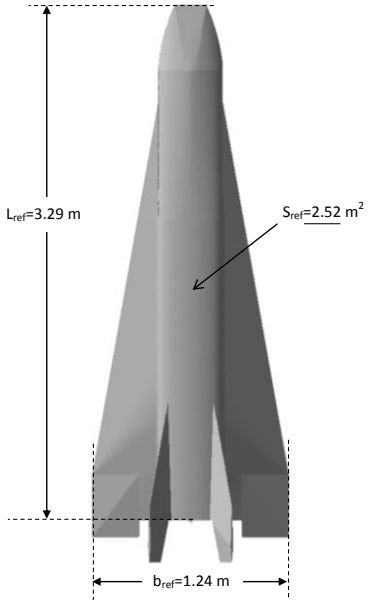

Figure 11. Reference quantities for EFTV aerodynamics.

B. Aerodynamic force and moments definitions and signs rules

In Figure 12 the adopted reference frame (BRF) with aerodynamic coefficients conventions are shown. The reference system for the aerodynamic data is a body-fixed axis system, compliant with the ISO 1151 standard.

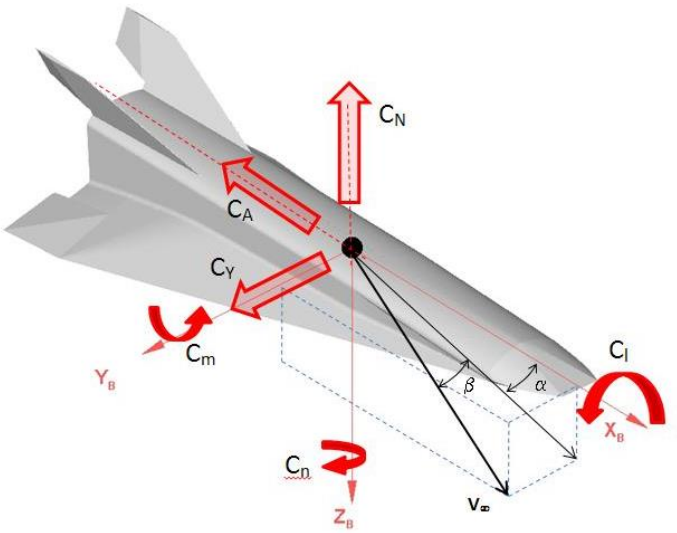

Figure 12. Reference frame and aerodynamic coefficients convention.

Directions of force and moment coefficients on the figure are positive as shown in Figure 12. The following aerodynamic sign convention for forces, moments, velocities, and accelerations is adopted (see Figure 10 and Figure 12): Angle of attack (α) is positive when free stream arrives from down of the pilot; Sideslip angle (β) is positive when free stream arrives from right of the pilot; Aileron deflection angle (δ_a) is positive when trailing edge is down; Elevon deflection angle (δ_e) is positive when trailing edge is down; Rudder deflection angle (δ_r) is positive when trailing edge

turns to the left of the pilot; Axial force coefficient (C_A) is positive when force is pushing in front of vehicle toward the base; Normal force coefficient (C_N) is positive when force is pushing on belly side of vehicle toward up; Side force coefficient (C_Y) is positive when force is pushing on left side of vehicle toward the right; Rolling moment coefficient (C_l) is positive when right wing is down; Pitching moment coefficient (C_m) is positive when the aircraft puts the nose up; Yawing moment coefficient (C_n) is positive when right wing is backward. Note that this is the convention usually adopted in Flight Mechanics.

For the sake of clarity, additional illustrations about aerodynamic sign convention are also provided in Figure 13.

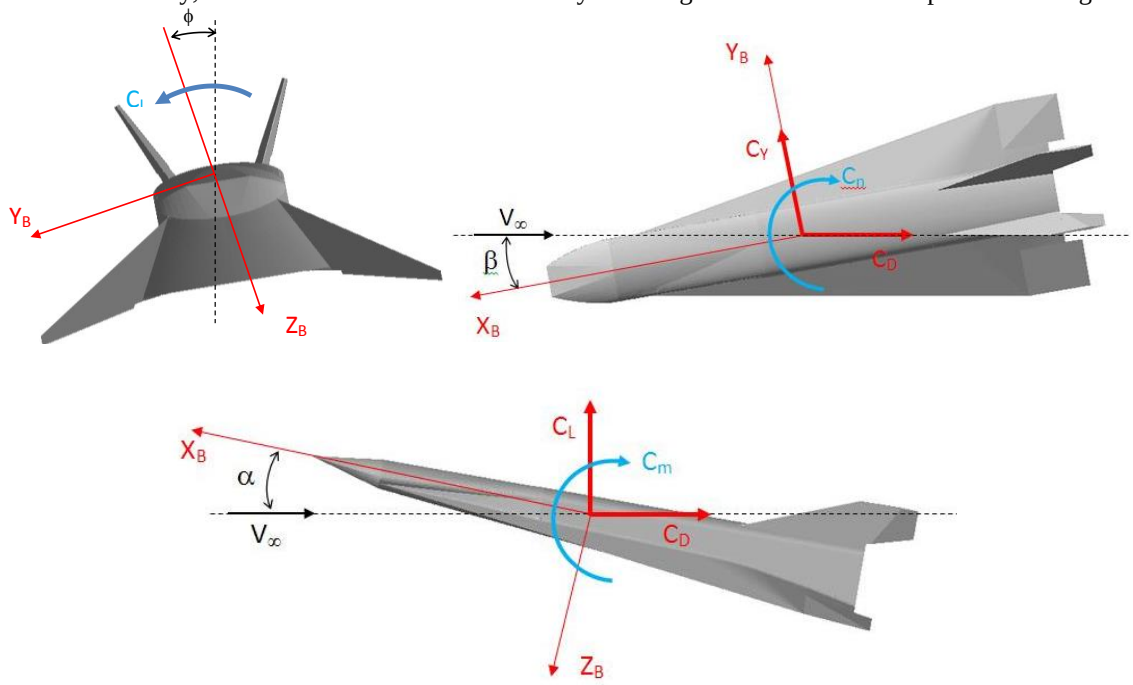

Figure 13. Aerodynamic coefficients convention and sign rule.

Therefore the aerodynamic static stability conditions, expressed in terms of derivatives, are the following: $C_{m\alpha}<0$, for longitudinal stability; and $C_{Y\beta}<0$, $C_{n\beta}>0$, $C_{l\beta}<0$, for lateral-directional stability.

C. Glider aerodynamic assessment in clean configuration

The aerodynamic data of EFTV presented in this paper are based upon inviscid CFD computations performed by DLR and Navier-Stokes simulations (both laminar and turbulent) carried out by CIRA, see paragraph V. G. This overview refers to EFTV aeroshape called FC4, i.e. the one used by DLR to build-up the full AEDB. The CFD matrix for the aerodynamic database includes 6 configurations for different aileron deflection angles δ and 80 different flow conditions defined by Mach number and angle of attack α. A sideslip angle β of 2 deg was also considered. Table 1 gives the CFD matrix condition in detail.

δ [°]	M [-]	α [°]	β [°]
-20 to +5 with Δδ =5	2 to 9 with ΔM=1	-6 to +12 with Δα=2	0 and 2

Table 1. Matrix of flow conditions and flap defections for the EFTV aerodynamic database.

In the following a few selected plots of the aerodynamic data set are shown. For instance, Figure 14 provides an overview of the lift and drag coefficients in function of Mach number with and without sideslip angle and aileron deflections effects. As shown, 2 deg sideslip angle does not change vehicle lift force, but negative aileron deflections (-5 and -10 in figure) significantly reduce the lift coefficient. For what concerns drag, Figure 14 points out that neither sideslip angle of 2 deg nor flap deflections of -5 and -10 deg determine considerable variation in drag. However, it is worth to note that these results refer to inviscid flowfield evaluations, i.e. the detrimental effect on aerodynamic performance of eventual local flow separations are not accounted for.

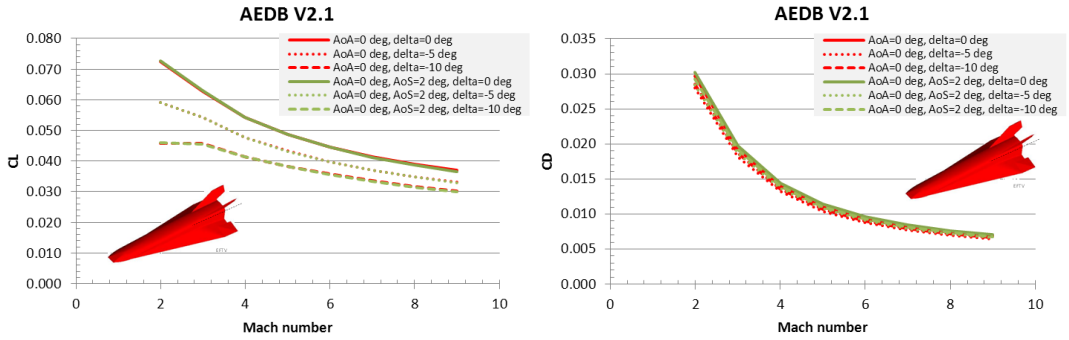

Figure 14. C_L and C_D vs. Mach number with and without sideslip angle and aileron deflection effects.

The same evaluation but for lift-to-drag ratio and pitching moment coefficient is summarized in Figure 15.

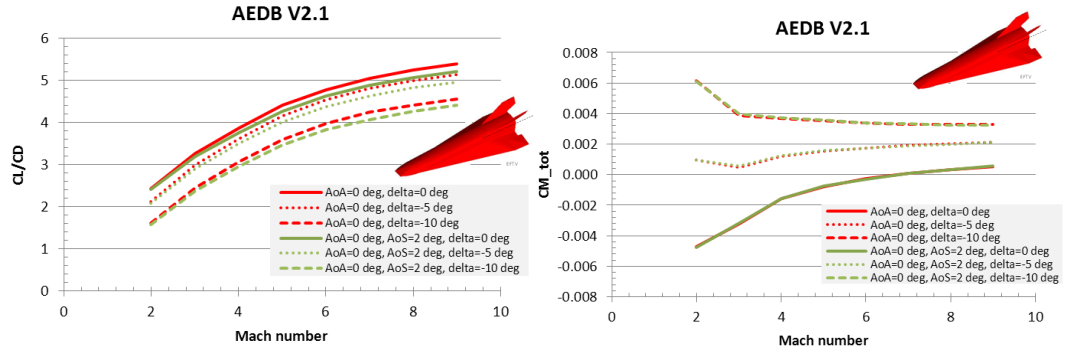

Figure 15. L/D and C_m vs. Mach number with and without sideslip angle and aileron deflection effects.

As one can see, the lift-to-drag ratio evolves accordingly to above suggestions for lift and drag, as shown in Figure 15. On the other hand, the pitching moment coefficient suggests that again 2 deg of sideslip flow does not markedly change C_m, but aileron deflections move upward the pitching moment characteristic, as expected. Note that in the Mach number range from 7 to 8, and AoA=0 deg, some conditions of natural trim (delta=0 deg) or trim obtained with a small positive aileron deflection (lower than 1 deg) are predicted.

The effect of aileron deflection on aerodynamic efficiency L/D at different angles of attack and at M_∞=2, 4, 6 and 8 is summarized in Figure 16.

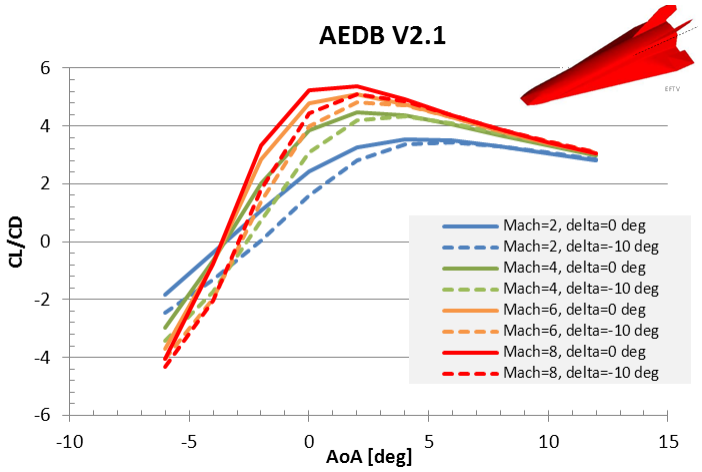

Figure 16. L/D vs. AoA at M=2, 4, 6, 8 and for 0 deg and -10 deg aileron deflections.

As shown, the aerodynamic efficiency is greater than 4 for Mach=6÷8 and AoA=-1÷7 deg. Anyway, some degradation of aerodynamic efficiency is expected when considering viscous effect evaluations.

D. Trim Conditions of the EFTV

The evolution of the pitching moment coefficient versus angle of attack for different Mach numbers (i.e. 2, 4, 6, and 8) and aileron deflections (i.e. 0, -5, -10, -15, and -20 deg) is summarized in Figure 17. For instance, Figure 17 points out that at M_∞=2 the EFTV aeroshape FC4 can be trimmed with proper aileron deflections from about -4 to 10 deg angle of attack. It is worth noting that pitching moment for 5 deg elevon deflection is not considered as no trim conditions are found for this flap setting.

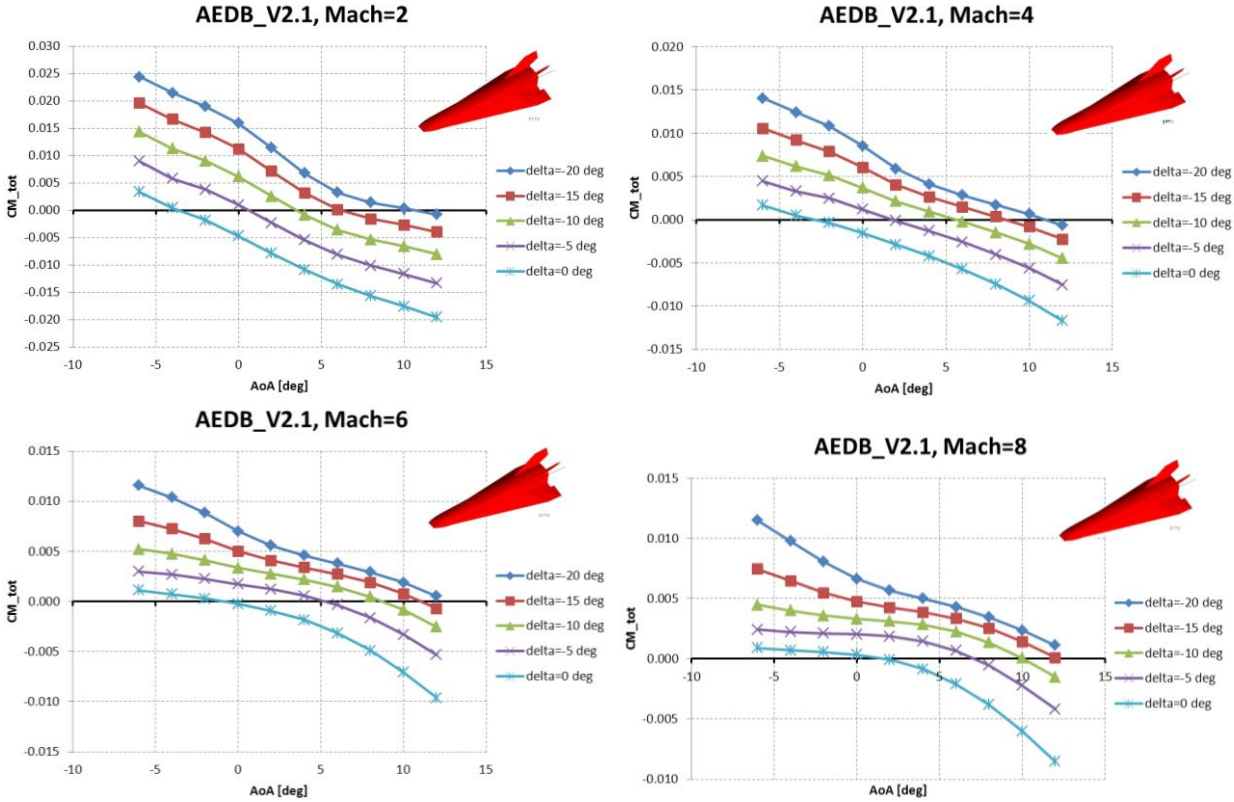

Figure 17. Pitching moment coefficient versus AoA at different aileron settings at M_∞=2, 4, 6, and 8.

At M_∞=4 Figure 17 shows that the trim range of AoA is about -3 to 11 deg; while at M_∞=6 and 8 these ranges are (-1, 12) deg and (2, 12) deg, respectively. Moreover, no significant effects of sideslip, for both clean and trimmed configurations are foreseen, as summarized in Figure 18.

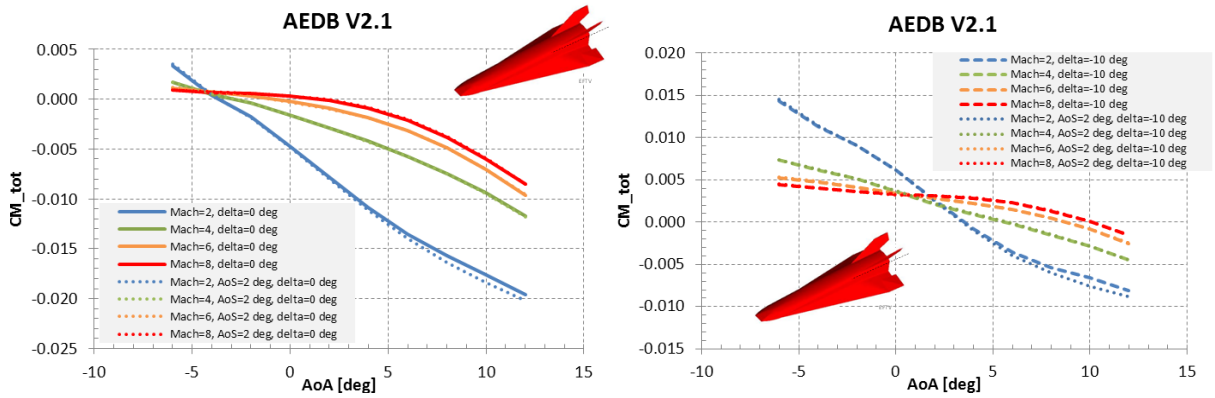

Figure 18. C_m versus AoA at different Mach numbers and with and without sideslip angle effects.

As a conclusive result, extracting data from AEDB V2.1 the aeroshape FC4 seems to be trimmable in all the flight conditions investigated, also for supersonic Mach numbers and higher angles of attack. Finally, the map of trim-ability

of EFTV is summarized in Figure 19. The effect of a sideslip angle of 2 deg is included as well, but it has been found to have no significant impact. Moreover, a typical "trimmed trajectory" including re-entry, pull-out manoeuvre and hypersonic glide phase (the black line with empty squares, reference trajectory) has been reported in the figure, showing clearly the trim capabilities characterizing the FC4 aeroshape.

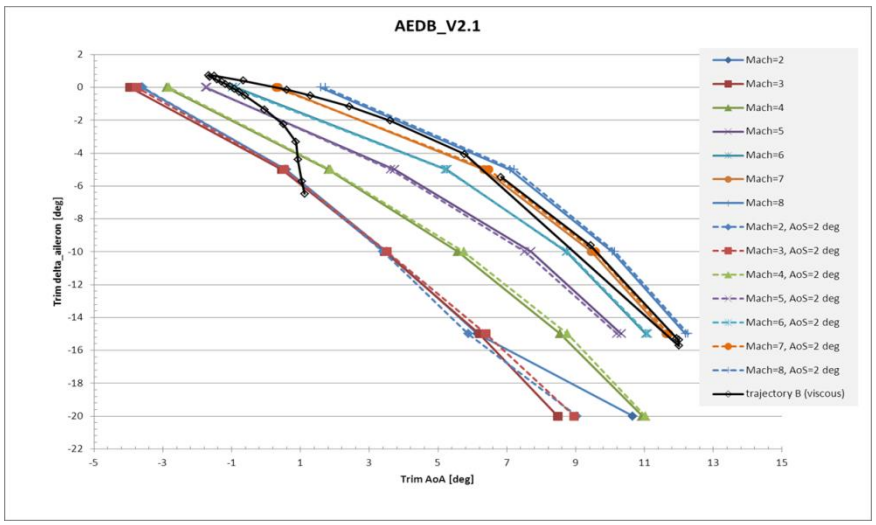

Figure 19. EFTV trim aileron deflection versus trim AoA at Mach numbers with and without 2 deg AoS.

E. Glider static stability in longitudinal and lateral-directional flight conditions

The slope of the pitching moment curve allows defining vehicle static stability conditions, i.e. $C_{m\alpha}<0$. Thus, Figure 17 and Figure 18 clearly underline that the glider is statically stable in longitudinal flight at all Mach numbers under investigation and for all the angles of attack, sideslip, and aileron deflections considered so far.

As far as static stability in lateral-directional flight conditions is concerned, recall that for side speed disturbance stability must be $C_{Y\beta}<0$. The physical meaning is: as a consequence of a positive side speed w disturbance a force is generated which tends to oppose w. Dihedral effect stability (i.e. static lateral stability) arises if $C_{l\beta}<0$. The instability physical meaning is: as a consequence of an angle of sideslip disturbance the airplane rolls towards the disturbance (increasing sideslip). To finish, weathercock Lateral Stability (static directional stability) needs for $C_{n\beta}>0$. Here the instability physical meaning is: as a consequence of an angle of sideslip disturbance the airplane flies away from the new relative wind.

The derivatives with respect to sideslip angle of side force, rolling moment and yawing moment coefficients at different Mach numbers and angles of attacks are summarized from Figure 20 to Figure 23. In particular, in Figure 20 the sideslip derivative of C_Y is provided. As shown, side speed disturbance stability (i.e. $C_{Y\beta}<0$) is predicted at all Mach numbers and AoAs here investigated.

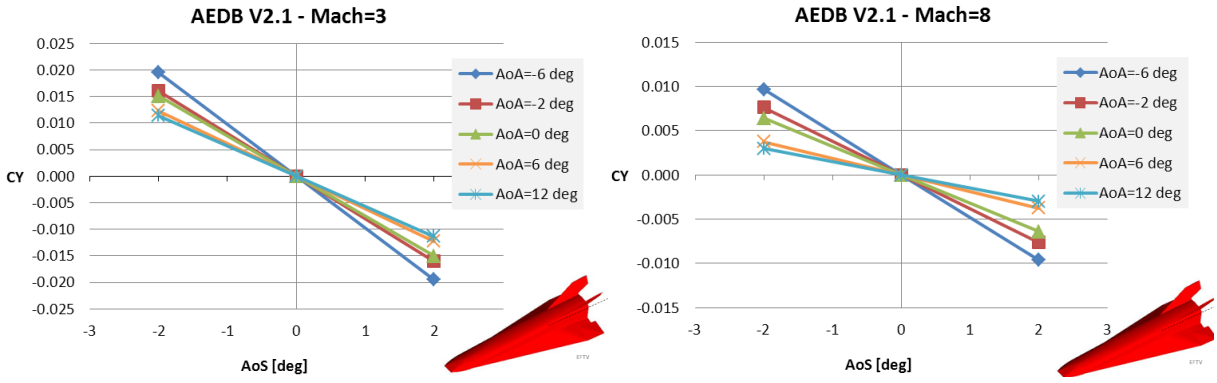

Figure 20. C_Y versus AoS at different AoA at M_∞=3 and 8.

The sideslip derivative of the rolling moment coefficient C_l is provided in Figure 21 at five angles of attack, namely -6, -2, 0, 6, and 12 deg. As one can see, dihedral effect stability is predicted at all Mach numbers for AoA ≥ 0 deg.

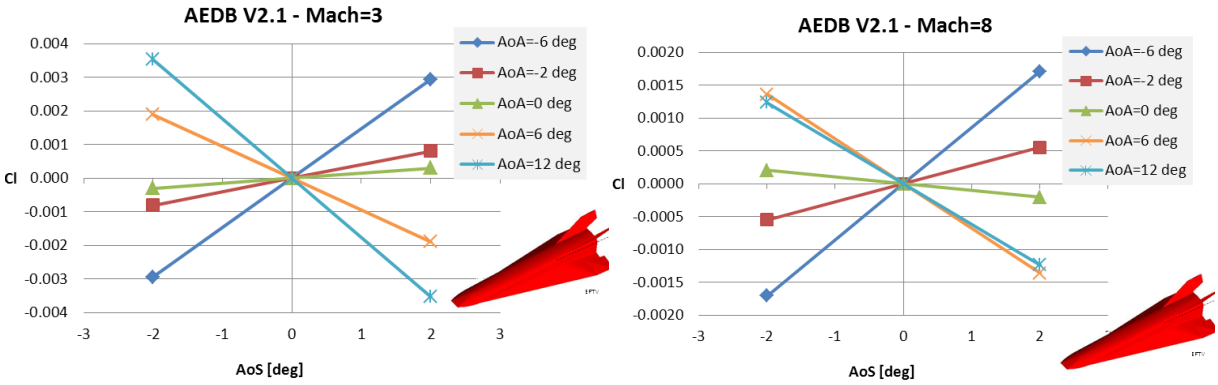

Figure 21. C_l versus AoS at different AoA at M_∞=3 and 8.

Finally, the sideslip derivative of the yawing moment coefficient C_n is provided in Figure 22 at five angles of attack, namely -6, -2, 0, 6, and 12 deg. As shown, the weathercock lateral stability is predicted at all Mach numbers and AoAs.

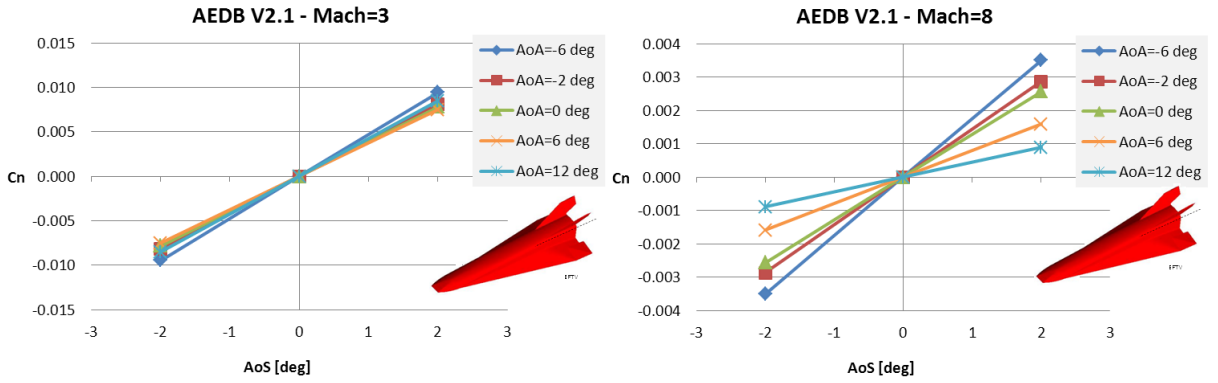

Figure 22. C_n versus AoS at different AoA at M_∞=3 and 8.

The effect of large yaw angles on sideslip derivatives of C_Y and C_n can be appreciated in Figure 23. As shown, no significant effects arise for yaw angle ranging from -8 to 8 deg.

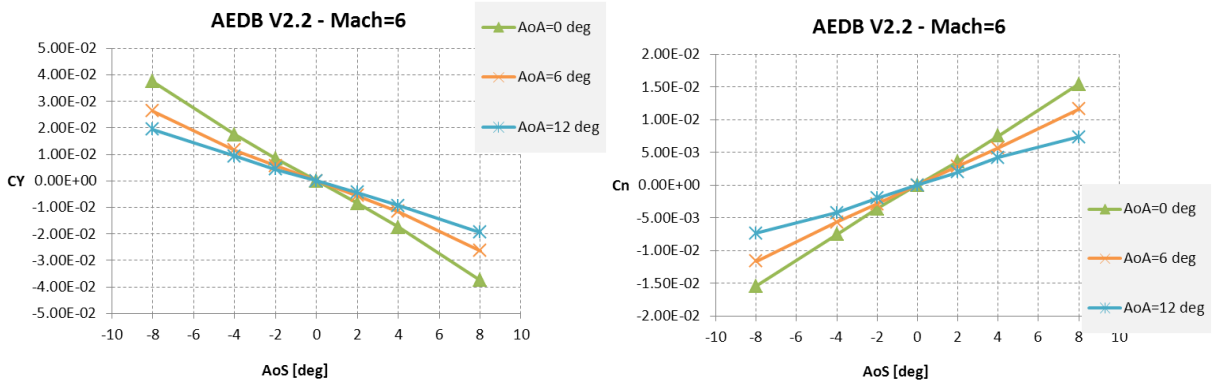

Figure 23. C_Y and C_n versus AoS at different AoA at M_∞=6. Effect of large yaw angles.

F. Glider hinge-line moments

Separate aerodynamic coefficients (forces and moments) have been computed for the ailerons with respect to the hinge line. The reference quantities are the same as for the full vehicle aerodynamics. As moment reference center, the center-point of the axis of rotation (flap hinge line) has been chosen, that is MRC_{flap}=(-2.588, 0.472, -0.247) [m]. In particular, hinge line moments for the aileron are provided for designing the actuation line and for selecting the actuator device itself.

The evaluation of hinge-moments (M_{hinge}) and flap normal forces (N_{flap}) at different aileron deflections, for all Mach numbers and at a maximum allowable dynamic pressure of 59 kPa (extracted by the reference trajectory), is summarized in Figure 24.

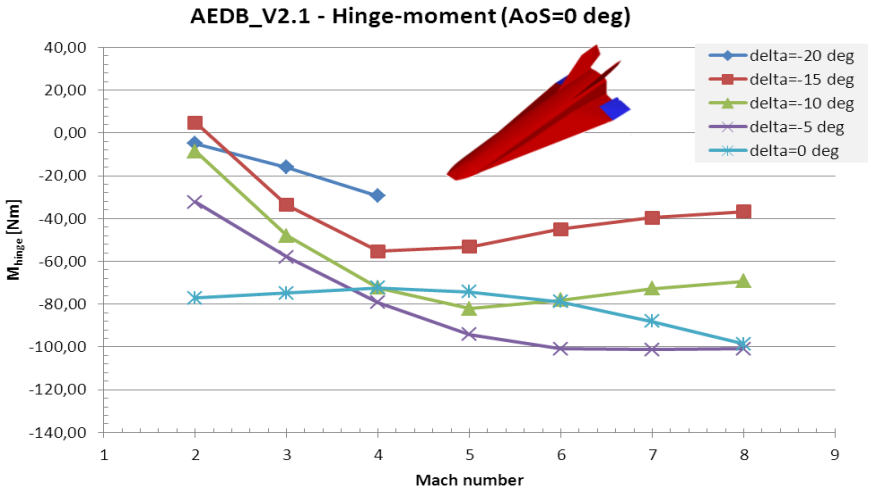

Figure 24. Hinge-moments at different aileron deflections, for all Mach numbers and at a maximum dynamic pressure of 59 kPa, AoS=0 deg.

The evaluation of flap normal forces (N_{flap}) and hinge-moments (M_{hinge}) in trimmed conditions for all Mach numbers is summarized in Figure 25.

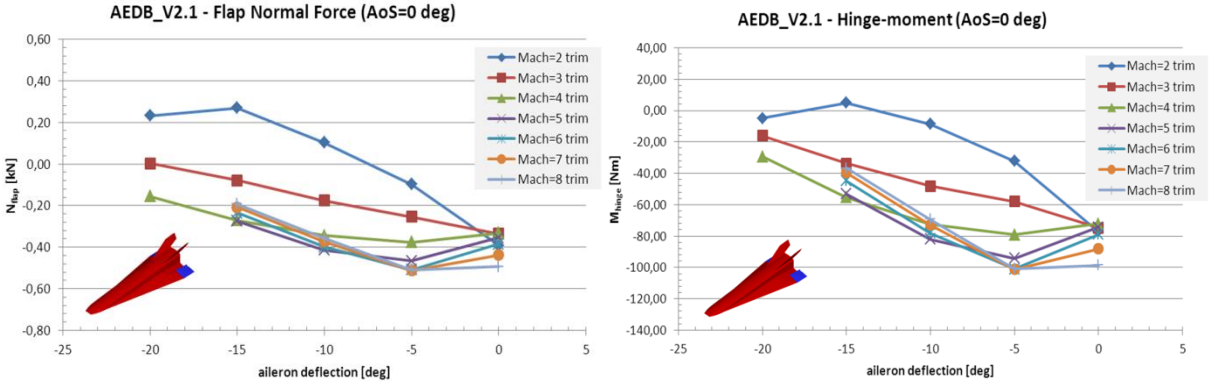

Figure 25. Flap normal force and hinge moments at each trim condition, for all Mach numbers and at AoS=0 deg.

As a conclusive result, ranging through all the possible trimmed conditions of FC4 aeroshape, M_{hinge} is in the range [-100÷5] Nm, while N_{flap} is in the range [-0.5÷0.25] kN. It is absolutely the case to underline here that these ranges will have to be verified by taking into account in CFD simulations the viscous effects and considering the uncertainties on aerodynamic estimations. Moreover, for the activation lane design and actuator selection also their mechanical and electrical-mechanical efficiencies, respectively, will have to be taken into account before to freeze design requirements.

Finally, hinge-moments versus time for the trimmed reference trajectory (namely, trajectory_B viscous) are summarized in Figure 26 together with time history of aileron trim angle. As one sees, along with the trimmed reference trajectory, M_{hinge} is in the range [-93÷-5] Nm and aileron trim angle is in the range [-15.72÷0.71] deg.

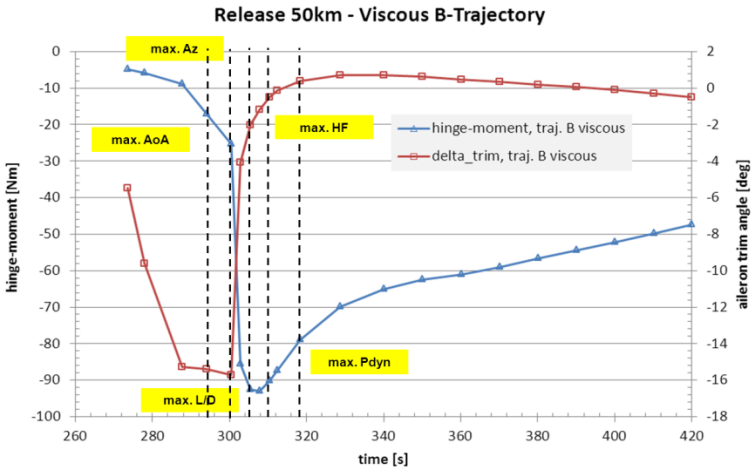

Figure 26. Hinge-moment and aileron trim deflection along the trimmed reference trajectory.

G. Glider viscous aerodynamics and coefficients breakdown

Preliminary Navier-Stokes computations of the flowfield past the glider have been carried out by CIRA at free-stream conditions selected along the reference trajectory summarized in Table 2, by using the numerical methodology described in paragraph IV.B

Point	explanation	Time [s]	Altitude [m]	Velocity [m/s]	Mach [-]	AoA [deg]	delta_trim [deg]
A	Max AoA	300.52	29936.43	2187.90	7.25	12.00	-15.72
B	Max $\dot{q}$	309.55	28040.09	2112.00	7.03	1.63	-0.68
C	Max L/D	305.49	28652.17	2136.93	7.10	3.62	-2.02

Table 2. Test Matrix of Navier-Stokes computations.

At these free-stream conditions, selected among the significant events along the trajectory (see Figure 26), CFD simulations (both in laminar and turbulent boundary layer assumptions) have been performed for radiative cooled wall (ε=0.4) boundary conditions considering unstructured hybrid grids as the one shown in Figure 27. Preliminary results are depicted in Figure 28, where are provided the Mach number field on symmetry plane and the pressure distribution on glider surface.

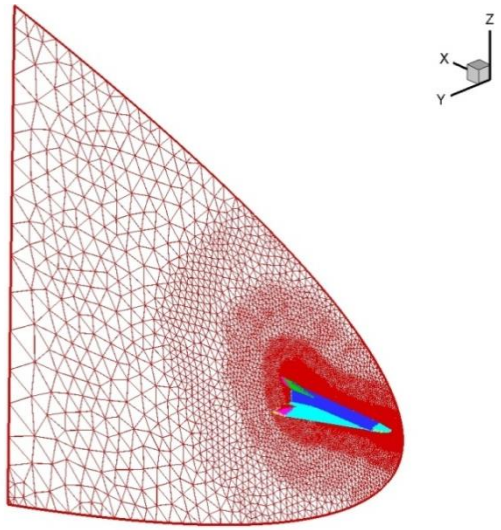

Figure 27. Typical CFD mesh domain (EFTV half configuration and symmetry plane).

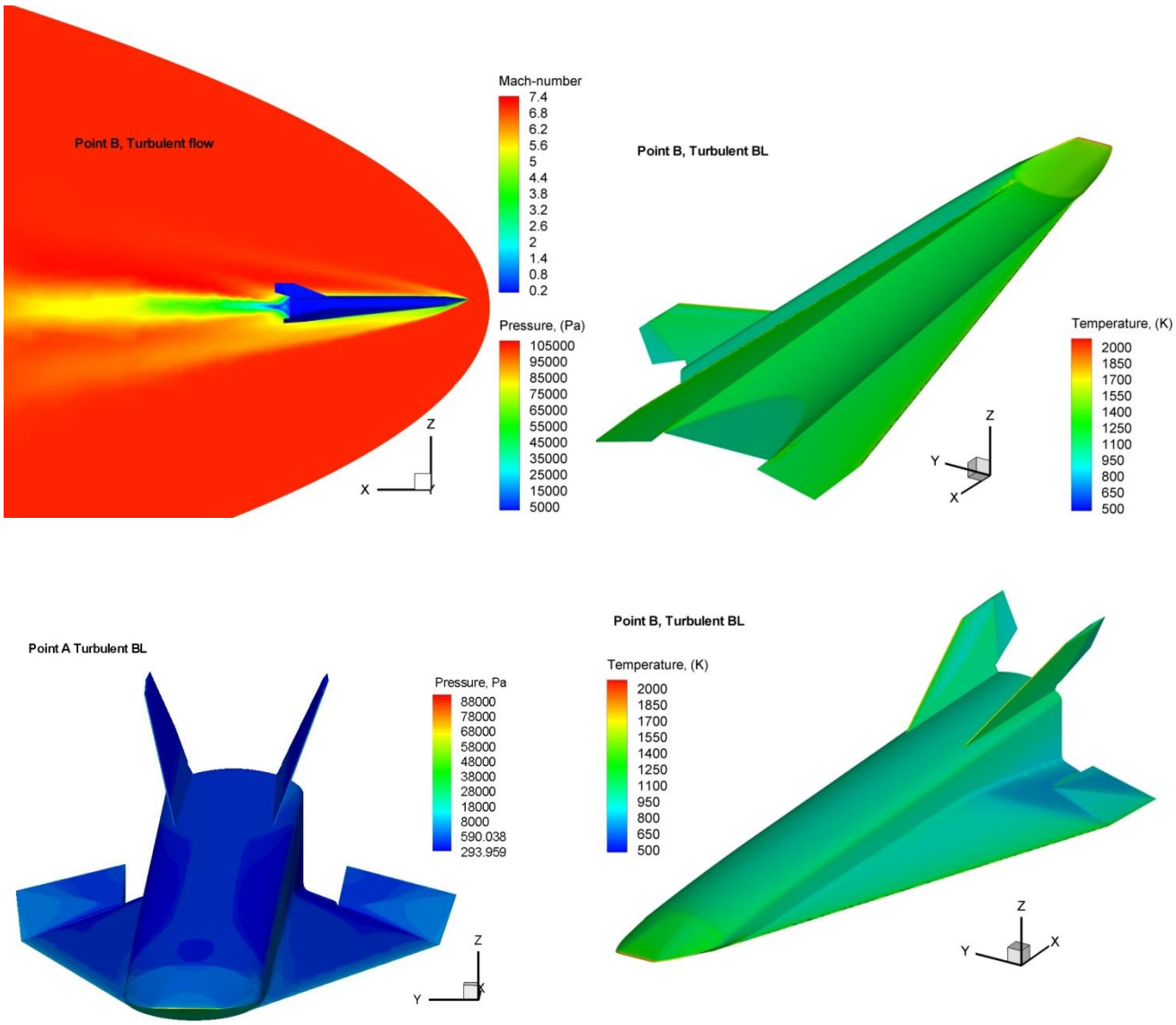

Figure 28. Mach number field on symmetry plane and pressure and temperature distributions on glider surface.

Results in terms of force and moment coefficients, for the flight points of Table 2, are summarized in Table 3, where also the "trimmed" aerodynamic coefficients (C_m=0) extracted by AEDB are reported for comparison purposes.

Note that the same aerodynamic coefficients used for the generation of reference trajectory have been reported here, i.e. the AEDB with the viscous correction only to axial force coefficient, based on the skin-friction coefficient evaluation for a compressible turbulent boundary layer using the reference temperature method. This has been done in order to cross-check the reliability of the method used in the trajectory generation. For instance, the estimate of the viscous forces acting on the vehicle has been obtained by treating the vehicle as a flat plate with a wetted area of 7.35m^2. So, the skin friction coefficient was evaluated for a compressible turbulent boundary layer using the reference temperature method.[9,10,11] For turbulent flow the skin friction coefficient is based on the correlation from Schoenherr, given by

$$C_f = 0.455 \frac{\rho_r}{\rho_e} log_{10}\left(\frac{\rho_r u_e L}{\mu_r}\right)^{-2.58} \tag{6}$$

where the subscript *r* refers to conditions that are evaluated at the turbulent reference temperature, and the subscript *e* refers to the free-stream conditions.[9] Note that the wall was assumed to be in radiative equilibrium with the surrounding atmosphere.

Point A	AoA	Source, Flow	C_A	C_N	C_m	C_D	C_L	C_L/C_D
	12	*CFD, Laminar*	0.02569	0.20861	-0.00036	0.06851	0.19871	2.90
	12	*CFD, Turbulent*	0.02825	0.21086	-0.00100	0.07147	0.20038	2.80
	12	*AEDB+vis.corr.*	0.02587	0.21064	0.0	0.06910	0.20065	2.90
Point B	AoA	Source, Flow	C_A	C_N	C_m	C_D	C_L	C_L/C_D
	1.63	*CFD, Laminar*	0.01222	0.05860	-0.00043	0.01389	0.05823	4.19
	1.63	*CFD, Turbulent*	0.01317	0.05954	-0.00058	0.01485	0.05914	3.98
	1.63	*AEDB+vis.corr.*	0.01374	0.05988	0.0	0.01544	0.05956	3.86
Point C	AoA	Flow	C_A	C_N	C_m	C_D	C_L	C_L/C_D
	3.62	*CFD, Laminar*	0.01356	0.08238	-0.00049	0.01873	0.08136	4.34
	3.62	*CFD, Turbulent*	0.01516	0.08347	-0.00068	0.02040	0.08234	4.04
	3.62	*AEDB+vis.corr.*	0.01512	0.08349	0.0	0.02036	0.08237	4.04

Table 3. Aerodynamic coefficients for Navier-Stokes computations.

By looking at the table, it can be said that the viscous correction to AEDB used to generate the reference trajectory has worked very well, as the values used for drag coefficient and aerodynamic efficiency are very similar to the ones predicted by CFD turbulent simulations (maximum differences lower than 4% on C_D and C_L/C_D). Consequently, also from the CFD simulations the EFTV has resulted practically trimmed for all the three flight conditions. Of course, the analysis has to be continued by comparing results for other nominal (along the "trimmed" trajectory) and off-nominal flight conditions.

Aerodynamic coefficient breakdowns are summarized from Figure 29 to Figure 31.

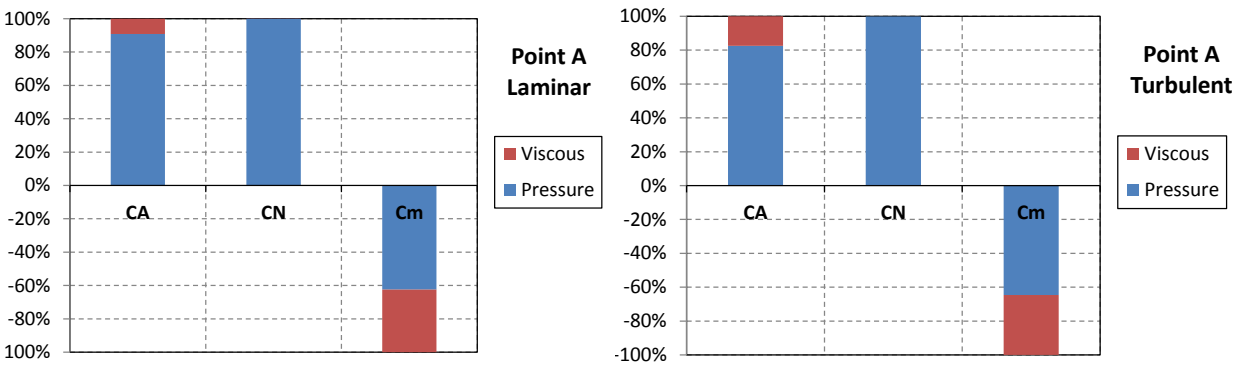

Figure 29. Point A, aerodynamic coefficients breakdown.

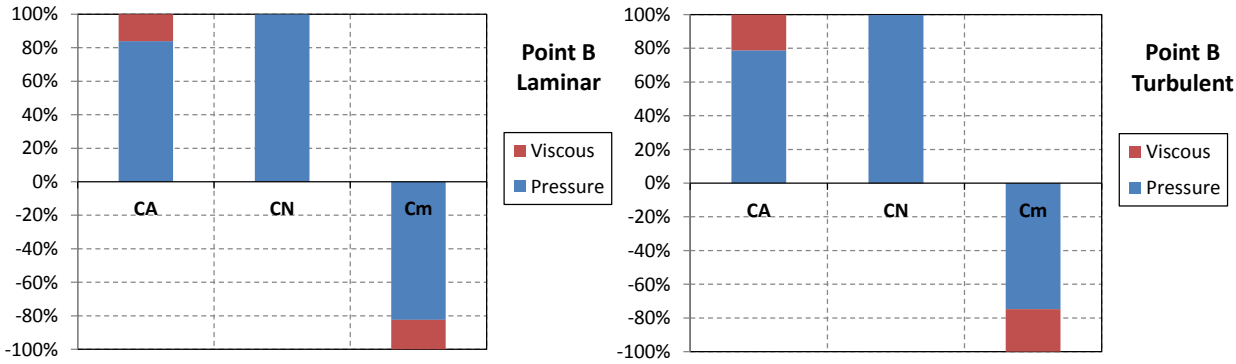

Figure 30. Point B, aerodynamic coefficients breakdown.

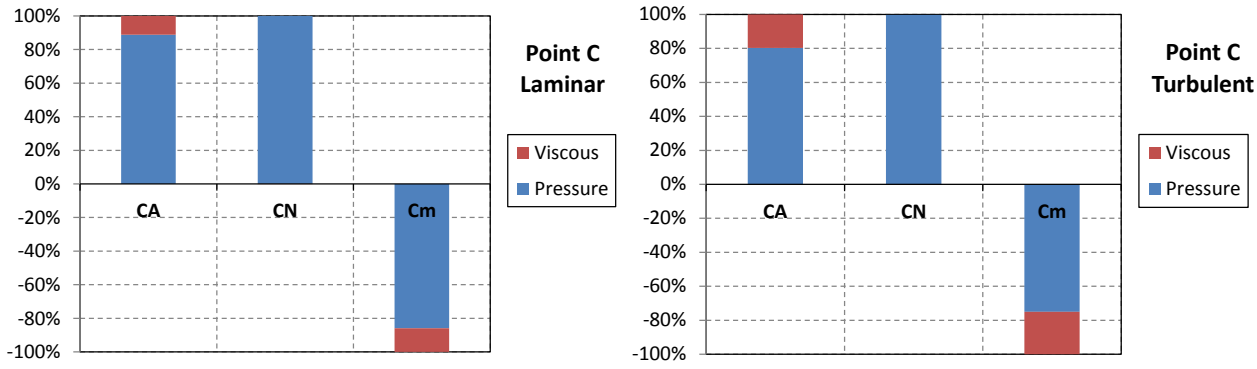

Figure 31. Point C, aerodynamic coefficients breakdown.

VI. Concluding Remarks

The present paper has dealt with the aerodynamic performance analysis of the experimental flight test vehicle under development in the seventh framework programme, namely HEXAFLY-INT. A mission scenario, the different flight segments and events to which the payload is exposed to have been described and justified. This has allowed for the definition of the aero-thermo-mechanical loads required to conceptually design all elements on board of the vehicle.

This flying test bed is a self-controlled glider configuration that shall face a levelled hypersonic flight at about Mach 8, just after the separation from the experimental support module at about 50 km altitude, up to the vehicle loss. During this flight several experiments shall be carried out. The appraisal of the vehicle aerodynamic performance is needed for Flight Mechanics and Guidance, Navigation and Control analysis. In particular, hinge line moments for the glider aileron have been also addressed to design the actuation lane and to select the actuator device itself. The vehicle design has made maximum use of databases, expertise, technologies and materials elaborated in previously European community co-funded projects ATLLAS I & II, LAPCAT I & II, and HEXAFLY.

Numerical results have pointed out the compliance of vehicle's aerodynamic performance with the flight envelope expected for the glider.

Aerodynamic results highlighted that vehicle aeroshape features a lift-to-drag ratio greater than 4 for Mach ranging from 6 to 8 and angle of attack from -1 to 7 deg. No significant effects of sideslip on aerodynamic efficiency, total pitching moment and map of trim-ability have been predicted. Moreover, the glider is statically stable both in longitudinal and lateral-directional flight conditions with the provided moment reference point for positive angles of attack, and is trimmable in pitch in all the flight conditions investigated in the present research effort.

Moreover, the first Navier-Stokes CFD simulations along three flight points of the trajectory (altitude 30 km, 28.6 km and 28 km) have shown that the viscous correction to AEDB used to generate the reference trajectory has worked very well, as the values used of drag coefficient and aerodynamic efficiency are very similar to the ones predicted by CFD turbulent simulations (maximum differences lower than 4% on C_D and C_L/C_D). Consequently, also from the CFD simulations the EFTV has resulted practically trimmed for these flight conditions.

Next steps consist in further iterating the trajectory with a more populated AEDB.

VII. Acknowledgments

This work was performed within the 'High-Speed Experimental Fly Vehicles-International' project fostering International Cooperation on Civil High-Speed Air Transport Research. HEXAFLY-INT, coordinated by ESA-ESTEC, is supported by the EU within the 7th Framework Programme Theme 7 Transport, Contract no.: ACP0-GA-2014-620327. Further info on HEXAFLY-INT can be found on http://www.esa.int/hexafly-int.

References

1. Steelant J., "European Activities on High-Speed Vehicles: Feasibility Studies and Technological Challenges for Hypersonic Cruisers", Aerothermodynamics Conference ATD7, ATD7-215019, May 2011, Bruges, Belgium.

2. Steelant, J., Varvill R., Defoort S., Hannemann K. and Marini M., "Achievements Obtained for Sustained Hypersonic Flight within the LAPCAT-II project", 20th AIAA International Space Planes and Hypersonic Systems and Technologies Conference, July Glasgow, Scotland. 2015.

3. Steelant J., "ATLLAS: Aero-Thermal Loaded Material Investigations for High-Speed Vehicles", 15th AIAA International Space Planes and Hypersonic Systems and Technologies Conference, 28/04-01/05-2008, Dayton, Ohio, USA, AIAA-2008-2582.

[4] Favaloro, N., Pezzella, G., Carandente, V., Scigliano, R., Vitale, A., Rispoli, A., Steelant, J., "Design Analysis of the High-Speed Experimental Flight Test Vehicle HEXAFLY-International", 20th AIAA International Space Planes and Hypersonic Systems and Technologies Conference, July Glasgow, Scotland. 2015.

[5] Pezzella G., Marini M., Cicala M., Vitale A., Langener T., Steelant J., "Aerodynamic Characterization of HEXAFLY Scramjet Propelled Hypersonic Vehicle", 32nd AIAA Applied Aerodynamics Conference, AIAA-2014-2844, Aviation 2014, 16-20 June 2014, Georgia, Atlanta, USA.

[6] Steelant J. et al., "Conceptual Design of the High-Speed Propelled Experimental Flight Test Vehicle HEXAFLY", 20th AIAA International Space Planes and Hypersonic Systems and Technologies Conference, July Glasgow, Scotland. 2015.

[7] Pezzella, G., van Brummen, S., Steelant, J., "Assessment of Hypersonic Aerodynamic Performance of the EFTV-ESM Configuration in the Framework of the Hexafly-INT Research Project", 8th European Symposium on Aerothermodynamics for Space Vehicles. 2-6 March. Lisbon. Portugal.

[8] Pezzella, G., Carandente, V., Scigliano, R., Marini, M., Steelant, J., Aerothermal Environment Methodology of the Hexafly-INT Experimental Flight Test Vehicle (EFTV)", 8th European Symposium on Aerothermodynamics for Space Vehicles. 2-6 March. Lisbon. Portugal.

[9] Walton,C., Cain, T., Trajectory analysis for the launch vehicle, ESM and EFTV, HEXAFLY-INT project Deliverable D6.3.1 February 2015.

[10] Anderson, J.D., Hypersonic and High Temperature Gas Dynamics, McGraw–Hill Book Company, New York, 1989.

[11] Bertin, J.J., Hypersonic Aerothermodynamics, AIAA Education Series, 1994.

[12] Viviani, A., Pezzella, G., Aerodynamic and Aerothermodynamic Analysis of Space Mission Vehicles. Springer International Publishing. DOI: 10.1007/978-3-319-13927-2. Hardcover ISBN 978-3-319-13926-5. eBook ISBN: 978-3-319-13927-2.

[13] Pezzella, G., "Hypersonic Aerothermal Environment Assessment of the CIRA FTB-X Reentry Vehicle". Aerospace Science and Technology, Volume 25, Issue 1, March 2013, Pages 190-202. http://dx.doi.org/10.1016/j.ast.2012.01.007.

[14] Schwamborn, D., Gerhold, T., Heinrich, R., "The DLR TAU-Code: Recent Applications in Research and Industry", ECCOMAS CFD 2006, Delft, The Netherlands, 2006